

# Three dimensional plasma arc simulation using resistive MHD

R. Jeltsch and H. Kumar

Research Report No. 2010-49  
December 2010

Seminar für Angewandte Mathematik  
Eidgenössische Technische Hochschule  
CH-8092 Zürich  
Switzerland

# THREE DIMENSIONAL PLASMA ARC SIMULATION USING RESISTIVE MHD

ROLF JELTSCH AND HARISH KUMAR

ABSTRACT. We propose a model for simulating the real gas, high current plasma arc in three dimension based on the equations of resistive MHD. These model equations are discretize using Runge-Kutta Discontinuous Galerkin (RKDG) methods. The Nektar code is used for the simulation which is extended to include Runge-Kutta time stepping, accurate Riemann solvers and real gas data. The model is then shown to be suitable for simulating plasma arc by using it to generate a high current plasma arc. Furthermore, the model is used to investigate the effects of the external magnetic field on the arc. In particular, it is shown that the external magnetic field forces the plasma arc to rotate.

## 1. INTRODUCTION

A circuit breaker is an electrical switch designed to protect electrical circuits from the damage that can be caused by high fault current or voltage fluctuations. Once a circuit breaker detects a fault, contacts within the circuit breaker open to interrupt the circuit. When the fault current is interrupted, a plasma arc is generated. This arc must be cooled, and extinguished in a controlled way, to protect connected circuits and the device itself. Hence, plasma arc provide a safe way of diffusing the energy of fault current. Consequently, the study of the arc behavior is of great importance to the power industry.

Many physical phenomenon occur during interruption of fault current in the circuit breaker, e.g. movement of contacts, pressure build up, radiative transfer, convection, heat conduction, melting of contact material, magnetic and electric effects. Due to the presence of these wide ranging phenomena, simulation of plasma arc is a difficult task. To overcome these difficulties extensive approximations related to the geometry, description of arc movements and the influence of magnetic fields on the plasma arc are made. Several authors propose models for the simulation of the plasma arc. In [1], authors present a three dimensional model for arc simulations at 100A current. In [2], effects of the external magnetic fields and the gas materials on a three-dimensional high current arc is simulated. However position of the arc root stay the same during temporal evolution and external magnetic field is imposed, not calculated. In [3] and [4], the external magnetic field is calculated using Biot-Savart law, and the arc root is not fixed.

The mathematical models proposed in [1],[2],[3],[4] are based on Navier-Stokes equations for fluid flow and Maxwell's equations for the electromagnetism which are solved simultaneously. They are coupled by adding the source terms in momentum balance due to Lorentz force and Joule heating in energy balance equation. These models although

suitable for small magnetic Reynolds number simulations, are highly unstable for large magnetic Reynolds number simulations.

In this work we are interested in developing a mathematical model for plasma arc with very high currents (100kA-200kA). At these high currents, very high temperatures are expected. This gives rise to high magnetic Reynolds number (in particular close to the contacts). Consequently, we consider a model based on equation of resistive magnetohydrodynamics (MHD). We believe that this is the first time a model based on resistive MHD has been used to simulate plasma arc in three dimensions (see [5],[6],[7]).

The equations of resistive magnetohydrodynamics (MHD) govern the evolution of a quasi-neutral conducting fluid and the magnetic field within it, neglecting the magnetization of individual particles, the hall current, ion slip and the time rate of change of the electric field in Maxwell's equations. The complete details about these equations can be found in [8]. Numerical discretization of these equations is complicated task due to the presence of nonlinearities in the convection flux. In addition to these difficulties, for the plasma arc simulations we need to consider a complicated geometry, real gas data for physical parameters, and mixed boundary conditions.

We use Runge-Kutta Discontinuous Galerkin (RKDG) methods for the discretization of MHD equations. Discontinuous Galerkin (DG) methods were first introduced by Hill and Reed in [9] for the neutron transport equations. These methods were then generalized for systems of hyperbolic conservation laws by Cockburn, Shu and co-workers (see [10]). In DG methods, the solution in space is approximated using piecewise polynomials on each element. Exact or approximate Riemann solvers from finite volume methods are used to compute the numerical fluxes between elements. Due to the assumed discontinuity of the solution at element interfaces, DG methods can easily handle adaptive strategies and can be easily parallelized.

To simulate plasma arc in the circuit breaker, we proceed as follows,

- (1) First, we assume that the domain is filled with hot gas. An arc is imposed between the contacts by specifying appropriate initial and boundary conditions.
- (2) This initial arc is then evolved till a steady state is reached. The principle idea is that with time, gas will radiate, which will result in temperature reduction everywhere except where gas is heated by the current in the arc. The resulting solution is now considered as an actual arc.
- (3) We then apply the external magnetic field by suitably modifying the magnetic field and the boundary conditions.
- (4) We show that using the appropriate external magnetic field it is possible to manipulate the arc. In particular, we show that the external magnetic field can be used to force the arc to rotate.

The article is organized as follows: In Section 2 we present the model equations of resistive MHD in non-dimensional variables. In Section 3 RKDG methods for resistive MHD equations in three dimensions is described. We present the variational formulation using a model equations. We then describe the three dimensional basis functions for different types of element. In Section 4, we first present initial and boundary conditions for arc

generations and discuss the simulation results. We then investigate the effect of external magnetic field on the arc.

## 2. EQUATIONS OF RESISTIVE MHD

For non-dimensional conservative variables, resistive MHD equations are,

$$\begin{aligned}
(1a) \quad & \frac{\partial \rho}{\partial t} + \nabla \cdot (\rho \mathbf{v}) = 0, \\
(1b) \quad & \frac{\partial(\rho \mathbf{v})}{\partial t} + \nabla \cdot \left( \rho \mathbf{v} \mathbf{v} - \mathbf{B} \mathbf{B} + \left( p + \frac{1}{2} |\mathbf{B}|^2 \right) \mathbf{I} - \frac{1}{Re} \Pi \right) = 0, \\
(1c) \quad & \frac{\partial \mathbf{B}}{\partial t} + \nabla \times \left( \mathbf{v} \times \mathbf{B} + \frac{1}{S_r} (\nabla \times \mathbf{B}) \right) = 0, \\
(1d) \quad & \frac{\partial E}{\partial t} + \nabla \cdot \left( (E + p) \mathbf{v} + \left( \frac{1}{2} |\mathbf{B}|^2 \mathbf{I} - \mathbf{B} \mathbf{B} \right) \cdot \mathbf{v} \right. \\
& \left. - \frac{1}{Re} \Pi \cdot \mathbf{v} + \frac{1}{S_r} \left( \mathbf{B} \cdot \nabla \mathbf{B} - \nabla \left( \frac{1}{2} |\mathbf{B}|^2 \right) \right) - \frac{1}{G_r} \nabla T \right) = ST^4 \\
(1e) \quad & \nabla \cdot \mathbf{B} = 0,
\end{aligned}$$

with the equation of state for energy,

$$(2) \quad E = \frac{p}{\gamma - 1} + \frac{1}{2} \rho |\mathbf{v}|^2 + \frac{1}{2} |\mathbf{B}|^2,$$

and the stress tensor,

$$(3) \quad \Pi = \nu \left( \nabla \mathbf{v} + (\nabla \mathbf{v})^\top \right) - \nu \frac{2}{3} (\nabla \cdot \mathbf{v}) \mathbf{I}.$$

Here  $\rho$  is the density,  $\mathbf{v}$  is the velocity,  $p$  is the pressure,  $\mathbf{B}$  is the magnetic field,  $E$  is the total energy and  $T$  is the temperature of the plasma. The Eqn. (1a) is the equation for the mass conservation. Eqns. (1a)-(1d) are equations of balance laws for the momentum, the magnetic field and the total energy respectively. Eqn. (1e) is the divergence free condition for magnetic field representing non-existence of magnetic monopoles.

The non-dimensionalization was carried out using the reference length  $L_0$ , the reference pressure  $P_0$  and the reference temperature  $T_0$ . Using these parameters, we use gas data to calculate the reference density  $\rho_0$  at temperature  $T_0$  and pressure  $P_0$ . Furthermore, the reference velocity is calculated using  $V_0 = \sqrt{P_0/\rho_0}$  and the reference magnetic field is calculated using,  $B_0 = \sqrt{P_0 \mu_0}$ , where  $\mu_0$  is magnetic permeability. The non-dimensional parameters appeared in the above equations are, Reynold number  $Re = \frac{\rho_0 V_0 L_0}{\nu}$ , Lundquist number  $S_r = \frac{\mu_0 V_0 L_0}{\eta}$ , Prandlt number  $G_r = \frac{\rho_0 V_0 L_0 R_0}{\kappa}$  and scaled Stefan's radiation constant  $S = \frac{s L_0 T_0^4}{V_0 P_0}$ . Here  $\nu$  is viscosity of the fluid,  $\eta$  ( $= 1/\sigma$ ) is the resistivity of fluid ( $\sigma$  is the conductivity of fluid),  $\kappa$  is the heat diffusion constant,  $R_0$  is the gas constant at temperature  $T_0$  and  $\gamma$  is the ratio of specific heats. In general, all of these quantities depends on the pressure and temperature. However we ignore their dependence on pressure. This is due to the negligible variation in these values due to the pressure change when compared to the variation due to the temperature change. Also,  $s$  is Stefan's radiation constant.

## 3. RKDG METHODS FOR RESISTIVE MHD

In this section we present spatial and temporal discretization of the MHD Eqns. (1). The spatial discretization is based on DG methods. Note that it is enough to consider DG methods for the scalar advection diffusion equation,

$$(4) \quad \frac{\partial u}{\partial t} + \sum_{1 \leq i \leq n} \frac{\partial}{\partial x_i} \left( f_i(u) - \sum_{i \leq j \leq n} a_{ij} \frac{\partial}{\partial x_j} u \right) = 0,$$

as we can apply the similar spatial discretization to each component of Eqns. (1). In Eqn. (4)  $f_i$  is convection flux,  $a_{ij}$  are diffusion coefficient with condition that matrix  $(a_{ij})_{ij}$  is symmetric and semi positive definite, so there exists a symmetric matrix  $(b_{ij})$  such that,

$$a_{ij} = \sum_{1 \leq l \leq d} b_{il} b_{lj}.$$

**3.1. Variational Formulation.** Following [10], we introduce a auxiliary variable  $q_l = \sum_{1 \leq j \leq n} b_{lj} \frac{\partial u}{\partial x_j}$  and rewrite the Eqn.(4) as,

$$(5a) \quad \frac{\partial u}{\partial t} + \sum_{1 \leq i \leq n} \frac{\partial}{\partial x_i} \left( f_i(u) - \sum_{i \leq l \leq n} b_{il} q_l \right) = 0,$$

$$(5b) \quad q_l - \sum_{1 \leq j \leq n} \frac{\partial g_{lj}}{\partial x_j} = 0, \text{ for } l = 1, \dots, n$$

where  $g_{lj} = \int_0^u b_{lj} ds$ . We set  $w = (u, q_1, q_2, \dots, q_n^\top)$ , and introduce the flux,

$$(6) \quad \mathbf{h}_i(w) = (f_i(u) - \sum_{1 \leq l \leq n} a_{il} q_l, -g_{1i}, \dots, -g_{ni})^\top.$$

Multiplying with test function and integrating by parts results in,

$$(7a) \quad \int_K \frac{\partial u}{\partial t} v_u dx - \sum_{1 \leq i \leq n} \int_K h_{iu} \frac{\partial}{\partial x_i} v_u dx + \int_{\partial K} \hat{h}_u(w, \mathbf{n}) v_h dx = 0,$$

$$(7b) \quad \int_K q_l v_{q_l} dx - \sum_{1 \leq j \leq n} \int_K h_{jq_l} \frac{\partial}{\partial x_j} v_{q_l} dx + \int_{\partial K} \hat{h}_{q_l}(w, \mathbf{n}) v_h dx = 0.$$

This is the variational formulation which we need to approximate. The flux  $\hat{\mathbf{h}}(w, \mathbf{n})$  is divided into two part,

$$\hat{\mathbf{h}} = \hat{\mathbf{h}}_{conv} + \hat{\mathbf{h}}_{diff}$$

where convective flux is given by,

$$\hat{\mathbf{h}}_{conv}(w^-, w^+, \mathbf{n}) = (\hat{f}(u^+, u^-, \mathbf{n}), 0)^\top.$$

Here  $\hat{f}$  is calculated using exact or approximated Riemann solvers. In these simulations we use local Lax-Friedrich numerical flux given by,

$$(8) \quad \mathbf{f}_{LF}(u^-, u^+) = \frac{1}{2} (f(u^-) + f(u^+)) - \frac{\max_i (\max(|\lambda_i(u^-)|, |\lambda_i(u^+)|))}{2} (u^+ - u^-),$$

where  $\lambda_i$  are eigenvalues of jacobian of MHD convection flux  $f$ . We use Bassi-Rebay flux (see [11]) to approximate the diffusion flux  $\hat{\mathbf{h}}_{diff}$ , i.e. the averages of diffusion fluxes across the interface.

**3.2. Three dimensional Basis functions.** The RKDG method we use is implemented in the Nektar code, developed by Karniadakis *et al.* (see [12, 13, 14]). The original code has been extended to include Runge-Kutta time stepping, slope limiters and accurate Riemann solvers, among other features (see [15]). In the DG discretization, functions are approximated by using basis functions:

$$(9) \quad f = \sum_i a_i \phi_i$$

where basis functions  $\phi_i$ 's are simple functions e.g polynomials. These functions are chosen in a way so that the whole algorithm is computationally efficient. The set of polynomial basis functions used in **Nektar** was proposed by Dubiner in [16] for two dimensions and extended to three dimensions in [12]. They are based on the tensor product of one dimensional basis functions which are derived using Jacobi polynomials. Here we describe three dimensional basis functions.

The one dimensional basis function are defined on bounded intervals, therefore an implicit assumption on the tensor product basis functions for higher dimension is that coordinates in two and three dimensional regions are bounded by constant limits. But in two or three dimension thats not true in general, e.g. triangle. To overcome this difficulty we define a collapsed coordinate system for three dimensions which maps elements without this property (Tetrahedral) to the element (Hexahedral) bounded by constant limits. These coordinates for various type of elements are given in Table 1.

Element Type	Upper Limits	Local Collapsed Coordinates		
Hexahedron	$-1 \leq \xi_1, \xi_2, \xi_3 \leq 1$	$\xi_1$	$\xi_2$	$\xi_3$
Prism	$\xi_1 \leq 1, \xi_2 + \xi_3 \leq 0$ with $-1 \leq \xi_1, \xi_2, \xi_3 \leq 1$	$\bar{\eta}_1 = \frac{2(1+\xi_1)}{1-\xi_2} - 1$	$\xi_2$	$\xi_3$
Pyramid	$\xi_1 + \xi_3, \xi_2 + \xi_3 \leq 0$ with $-1 \leq \xi_1, \xi_2, \xi_3 \leq 1$	$\bar{\eta}_1 = \frac{2(1+\xi_1)}{1-\xi_2} - 1$	$\eta_2 = \frac{2(1+\xi_2)}{1-\xi_2} - 1$	$\eta_3 = \xi_3$
Tetrahedron	$\xi_1 + \xi_2 + \xi_3 \leq -1$ with $-1 \leq \xi_1, \xi_2, \xi_3 \leq 1$	$\eta_1 = \frac{2(1+\xi_1)}{-\xi_2-\xi_3} - 1$	$\eta_2 = \frac{2(1+\xi_2)}{1-\xi_2} - 1$	$\eta_3 = \xi_3$

TABLE 1. Local collapsed coordinates for three dimensional elements.

Under these transformed coordinates, three dimensional elements are bounded by constant limits. For example tetrahedron  $\hat{T}_3$  which in Cartesian coordinates is given by,

$$\hat{T}_3 = \{-1 \leq \xi_1, \xi_2, \xi_3 \leq 1, \text{ such that } \xi_1 + \xi_2 + \xi_3 \leq -1\}$$

is transformed to,

$$\hat{T}_3 = \{-1 \leq \eta_1, \eta_2, \eta_3 \leq 1\}$$

in local collapsed coordinates. To define three dimensional basis function, we first define functions,

$$(10) \quad \psi_p^a(z) = P_p^{0,0}(z), \quad \psi_{pq}^b(z) = \left(\frac{1-z}{2}\right)^p P_q^{2p+1,0}(z),$$

$$(11) \quad \psi_{pqr}^c(z) = \left(\frac{1-z}{2}\right)^{p+q} P_r^{2p+2q+2,0}(z),$$

where  $P_n^{\alpha,\beta}$  is the  $n$ th-order Jacobi polynomial with weights  $\alpha$  and  $\beta$ . Then using local collapsed coordinates the three dimensional basis functions for various elements are given in Table 2.

Hexahedron Basis	$\phi_{pqr}(\xi_1, \xi_2, \xi_3) = \psi_p^a(\xi_1)\psi_q^a(\xi_2)\psi_r^a(\xi_3)$
Prism Basis	$\phi_{pqr}(\xi_1, \xi_2, \xi_3) = \psi_p^a(\bar{\eta}_1)\psi_q^a(\xi_2)\psi_{pr}^b(\xi_3)$
Pyramid Basis	$\phi_{pqr}(\xi_1, \xi_2, \xi_3) = \psi_p^a(\bar{\eta}_1)\psi_q^a(\eta_2)\psi_{pqr}^c(\eta_3)$
Tetrahedron Basis	$\phi_{pqr}(\xi_1, \xi_2, \xi_3) = \psi_p^a(\eta_1)\psi_{pq}^b(\eta_2)\psi_{pqr}^c(\eta_3)$

TABLE 2. Basis functions for Three dimensional Elements

These basis functions are orthogonal in the Legendre inner product over each element, resulting in a diagonal mass matrix. The functions are polynomial in both the Cartesian and non-Cartesian co-ordinates. It was proved in [17] that the coefficients of the basis functions in a solution decay exponentially with polynomial order, thus the numerical solution converges exponentially as the maximum polynomial order of the approximation is increased.

order	$\alpha_{il}$		$\beta_{il}$		
2	1		1		
	1/2	1/2	0	1/2	
3	1		1		
	3/4	1/4	0	1/4	
	1/3	0	2/3	0	0

TABLE 3. Parameters for Runge-Kutta time marching schemes.

**3.3. Time stepping.** To advance solutions in time, the RKDG method uses a Runge-Kutta (RK) time marching scheme. Here we present the second-, third- and fourth-order accurate RKDG schemes. For second- and third-order simulations, we present the TVD RK schemes of Shu (see [18]). For fourth-order simulations we use the classic scheme. Consider the semi-discrete ODE,

$$\frac{du_h}{dt} = L_h(u_h).$$

Let  $u_h^n$  be the discrete solution at time  $t^n$ , and let  $\Delta t^n = t^{n+1} - t^n$ . In order to advance a numerical solution from time  $t^n$  to  $t^{n+1}$ , the RK algorithm is as follows:

1. Set  $u_h^{(0)} = u_h^n$ .
2. For  $i = 1, \dots, k + 1$ , compute,

$$u_h^{(i)} = \sum_{l=0}^{i-1} \alpha_{il} u_h^{(l)} + \beta_{il} \Delta t^n L_h(u_h^{(l)}).$$

3. Set  $u_h^{n+1} = u_h^{(k+1)}$ .

The values of the coefficients used are shown in Table 3. For the linear advection equation, it was proved by Cockburn *et al.* in [19] that the RKDG method is  $L^\infty$ -stable for piecewise linear ( $k = 1$ ) approximate solutions if a second-order RK scheme is used with a time-step satisfying,

$$c \frac{\Delta t}{\Delta x} \leq \frac{1}{3},$$

where  $c$  is the constant advection speed. The numerical experiments in [10] show that when approximate solutions of polynomial degree  $k$  are used, an order  $k + 1$  RK scheme must be used, which simply corresponds to matching the temporal and spatial accuracy of the RKDG scheme. In this case the  $L^\infty$ -stability condition is

$$c \frac{\Delta t}{\Delta x} \leq \frac{1}{2k + 1}.$$

For the nonlinear case, the same stability conditions are used but with  $c$  replaced by the maximum eigenvalue of the system.

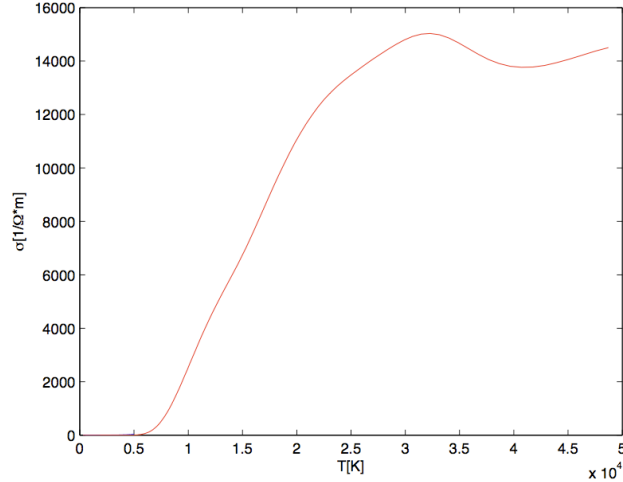


FIGURE 1. Conductivity of the  $SF_6$  gas at pressure  $P = 10^6$  Pa

#### 4. THREE DIMENSIONAL ARC SIMULATIONS

To simulate the plasma arc, the Nektar code has been modified to implement real gas data for following physical parameters: conductivity, fluid viscosity, specific heats, gas constant and thermal conductivity. The gas used in circuit breakers is  $SF_6$ . The real gas data is implemented by approximating it at pressure  $10^6$  Pa, with smooth functions (see [6, 7]). An example of this is given in Fig. 1, where we have plotted the approximated electrical conductivity w.r.t. temperature. Note that, the dependence of the gas data on temperature introduces further stiffness in the equations. All the results presented here are of first order accuracy.

The domain for simulation is illustrated in Figs. 2. In Fig. 2(a) we have the three dimensional domain for the computation which is the arc chamber of the circuit breaker. Fig. 2(b) shows  $XY$  plane cut of the three dimensional geometry. The domain is axial symmetric along the  $y$ -axis. The radius of domain is  $70$  mm and length ( $y$ -axis) is  $200$  mm long. We assume that we have an arc attached to both electrodes which are  $10$  mm wide.

In a circuit breaker with rotating arc, the current that flows inside the arc also goes through a coil located around the arc chamber. This process induces an external magnetic field in the  $y$ - direction. This external magnetic field interacts with the arc through the Lorentz force term in the momentum conservation equation. Observe that, in the design of arc chamber, the contacts at the arc root have different radii, which guarantees that the current in the resulting arc will not be parallel to  $y$ -axis. Consequently, the Lorentz force term  $\mathbf{J} \times \mathbf{B}$  will be nonzero.

**4.1. Arc generation.** Initially, we assume that the domain (see Fig. 2) is filled with,  $SF_6$  gas at the temperature of  $20000$  K and the pressure  $10^6$  Pa. At these values of pressure and temperature, the density of the  $SF_6$  gas is,  $0.0829 Kg/m^3$ . The flow is considered to be

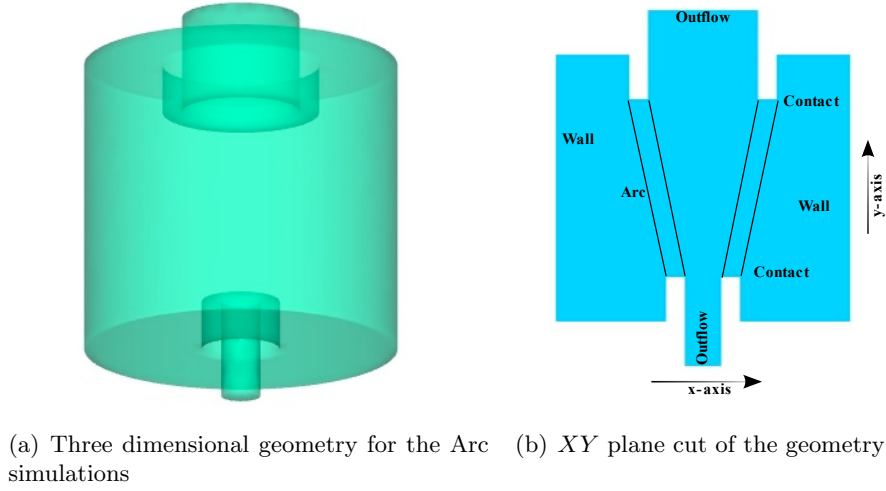


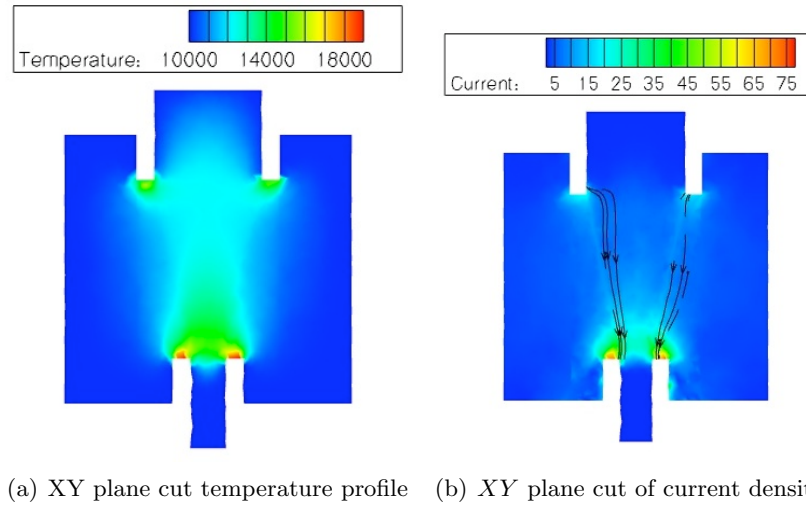
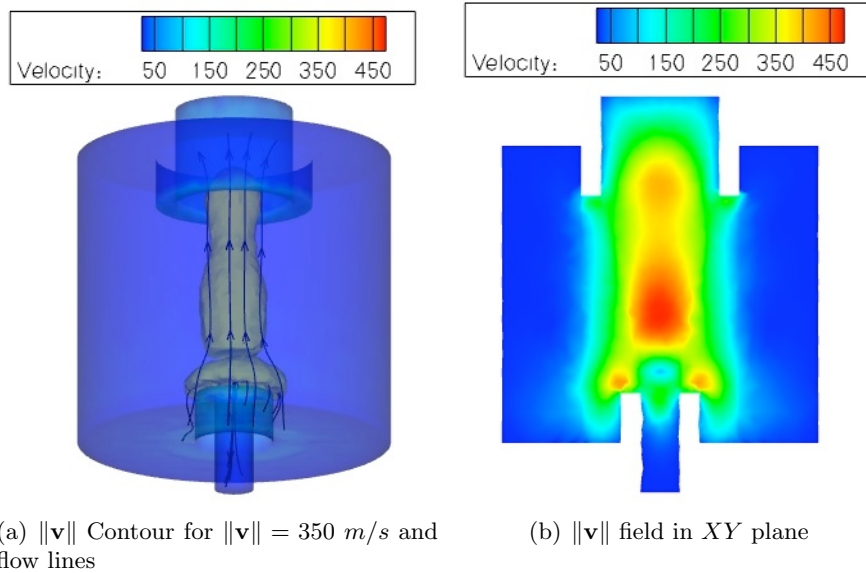
FIGURE 2. Geometry of the Arc chamber

steady initially, i.e.  $\mathbf{v} = 0.0$  m/s. The magnetic field components  $B_x$  and  $B_z$  are computed using *Biot-Savart Law* and corresponds to the total current of  $I = 100$  kA in the initial arc of width 10mm (see [6, 7]) joining both contacts.

We consider the reference length of  $L_0 = 10^{-3}$  m. The reference pressure is  $P_0 = 10^6$  Pa, and the reference temperature is  $T_0 = 5000$  K. Using the gas data, we have the reference density  $\rho_0 = 0.506$  kg/m<sup>3</sup>. Wall boundary condition for the wall are the same as in the previous chapter. Wall temperature is  $T = 10000$  K except at the arc roots where we put  $T = 20000$  K. Wall boundary conditions are implemented for velocity by inverting the normal component of velocity at the wall. Magnetic field conditions for the wall are implemented by assuming condition of no current.

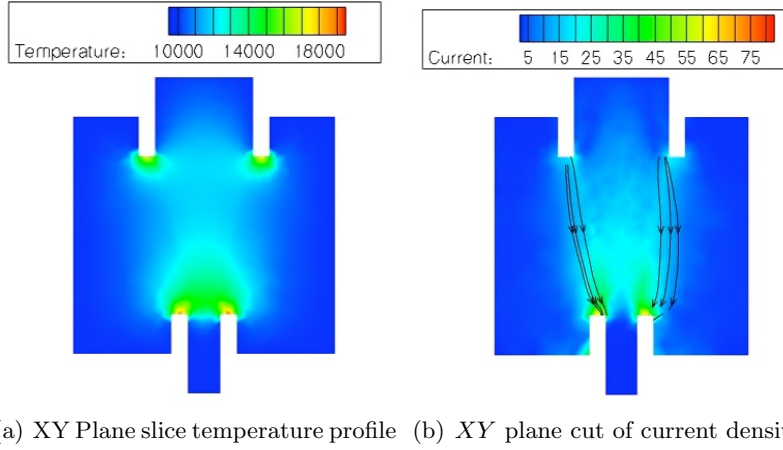
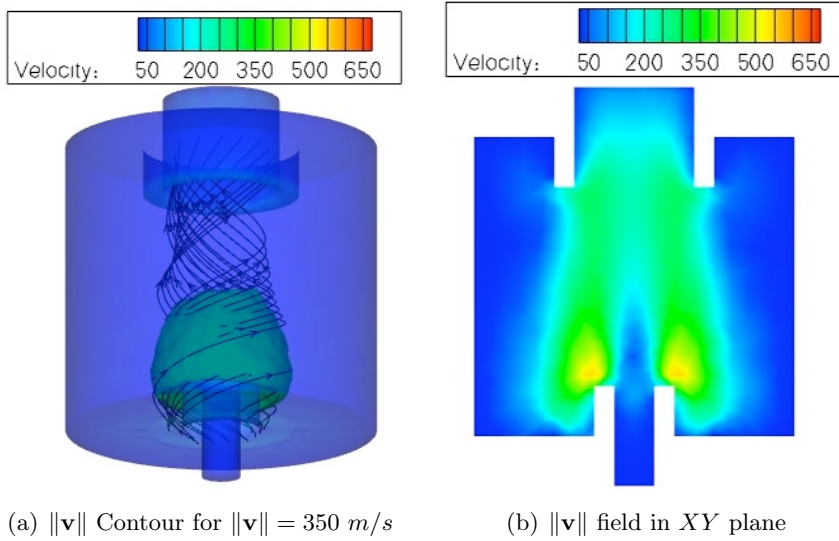
Using these reference variables and assuming that the minimum conductivity is  $\sigma_{min} = 6000$ , we would have a *Lundquist* number  $S_r = \mu_0 V_0 L_0 \sigma_{min} = 1.06 \times 10^{-2}$ . This value would give rise to an extremely stiff system and this in turn would make the computational time unreasonably large. We scale this with a factor of 1000. Similarly, we scale  $G_r$  with a factor of 20. We do realize that this can effect results quantitatively, but we believe that qualitatively the results still hold. We use 101044 tetrahedron elements in our computations. Computational time is 24 hours with 64 processors. At time  $t = 0.569$  ms we have the following results:

Fig. 3(a) is the temperature profile of the arc in XY plane. We observe that most of the heating takes place at the center of the domain. Fig 3(b) is the current density profile of the arc in XY plane with the current lines and the current moving downward. The current lines has moved towards the center of the domain from its initial position due to higher temperature. Fig. 4(b) is the profile of the velocity field. We also note that the gas is

FIGURE 3. Temperature and current density at time  $t = 0.569 \text{ ms}$ FIGURE 4.  $\|\mathbf{v}\|$  field of the arc at  $t = 0.569 \text{ ms}$ 

pushed away from the arc, through the outflow boundaries. There is also a bifurcation in velocity flow lines near the lower end of the domain.

**4.2. Effects of external magnetic fields.** The external magnetic field of  $B_y = 0.5 \text{ T}$  is applied by adding it to the arc's magnetic field and then modifying the boundary conditions

FIGURE 5. Temperature with external magnetic field after time  $t = 1.138 \text{ ms}$ FIGURE 6.  $\|\mathbf{v}\|$  field with external magnetic field after time  $t = 1.138 \text{ ms}$ 

with the magnetic field  $B_y = 0.5 \text{ T}$ . Note that, during the simulations,  $y$ -component  $B_y$  of the magnetic field is also simulated. The computational time was another 24 hours on 64 processors. After further  $t = 0.569 \text{ ms}$ , we obtain the following results:

Fig. 5(a) illustrate temperature profile of the arc. We observe that, the temperature is comparatively less than what it was before. Fig. 5(b) represent the new current density profile. When compared with Fig. 3(b) we observe that there is a change in the shape of the current density close to the lower contact. The most important result is shown in

Fig. 6. The streamlines of the velocity field show that the arc is rotating. In fact, the velocity profile is completely changed when compared with the Fig. 4. Also, note the significant jump in the absolute value of the velocity. Without the external magnetic field the maximum absolute velocity was  $490\text{ m/s}$ , compared to  $689\text{ m/s}$  with external magnetic field. Furthermore, the maximum velocity is at the arc roots, instead of at the center.

## 5. CONCLUSION

We show the suitability of the equations of resistive MHD for three dimensional computations of the plasma arc in high current circuit breakers. These equations are used to generate the arc for a total current of  $100\text{ kA}$ . We then apply the external magnetic field and use it to generate a rotation in the arc and observe a significant increase in the velocity. This can be used to minimize the operating energy of the circuit breaker. One of the major obstacle in simulating the real gas arc is the stiffness due to the low values of the conductivity. A possible solution for this can be use of implicit time stepping for the simulations.

**Acknowledgement.** The authors would like to acknowledge C. Schwab, V. Wheatley, M. Torrillon and R. Hiptmair for their support and constructive discussions on this work. G. E. Karniadakis provided the authors with the original version of Nektar and ABB Baden provided real gas data for  $SF_6$  gas, which is gratefully acknowledged.

## REFERENCES

- [1] SCHLITZ, L. Z. AND GARIMELLA S. V. AND CHAN, S. H., *Gas Dynamics and electromagnetic processes in high-current arc Plasmas. Part I Model Formulation and steady state solutions*, Journal of Applied Physics, Vol. 85(5) (1999), pages 2540-2546.
- [2] SCHLITZ, L. Z. AND GARIMELLA, S. V. AND CHAN, S. H., *Gas Dynamics and electromagnetic processes in high-current arc Plasmas. Part II Effects of external magnetic fields and gassing materials*, Journal of Applied Physics, Vol. 85(5) (1999), pages 2547-2555.
- [3] LINDMAYER, M., *Simulation of switching devices based on general transport equation*, Int. Conference on Electrical Contacts, Zurich (2002).
- [4] BARCIKOWSKI, F. AND LINDMAYER, M., *Simulations of the heat balance in low-voltage switchgear*, Int. Conference on Electrical Contacts, Stockholm (2000).
- [5] HUGUENOT P., KUMAR H., WHEATLEY V., JELTSCH R., SCHWAB C., *Numerical Simulations of High Current Arc in Circuit Breakers*, 24th International Conference on Electrical Contacts (ICEC) (2008), Saint-Malo, France.
- [6] HUGUENOT, P., *Axisymmetric high current arc simulations in generator circuit breakers based on real gas magnetohydrodynamics models*, Diss., Eidgenössische Technische Hochschule ETH Zrich (2008), No. 17625.
- [7] KUMAR, H., *Three Dimensional High Current Arc Simulations for Circuit Breakers Using Real Gas Resistive Magnetohydrodynamics*, Diss., Eidgenössische Technische Hochschule ETH Zrich (2009), No. 18460.
- [8] GOEDBLOED, H. AND POEDTS, S., *Principles of Magnetohydrodynamics*, Cambridge University Press (2004).
- [9] HILL, T. R., REED W. H., *Triangular mesh methods for neutron transport equation*, Tech. Rep. LA-UR-73-479, Los Alamos Scientific Laboratory, 1973.

- [10] COCKBURN B., *Advanced Numerical Approximation of Nonlinear Hyperbolic Equations*, Chapter *An introduction to the Discontinuous Galerkin method for convection-dominated problems*, Lecture Notes in Mathematics, Springer (1998), pages 151-268.
- [11] BASSI, F. AND REBAY, S., *A high-order accurate discontinuous finite element method for the numerical solution of the compressible Navier-Stokes equations*, J. Comp. Phys., Vol. 131 (1997), pages 267-279.
- [12] SHERWIN, S. J. AND KARNIADAKIS, G. E., *A new triangular and tetrahedral basis for high-order(hp) finite element methods*, Int. J. Numer. Methods. Eng., Vol. 123 (1995), pages 3775-3802.
- [13] KARNIADAKIS, G. E., AND SHERWIN, S. J., *Spectral/hp Element Methods for Computational Fluid Dynamics*, Oxford University Press (2005).
- [14] LIN, G. AND KARNIADAKIS, G. E., *A discontinuous Galerkin Method for Two-Temperature Plasmas*, Comp. Meth. in Appl. Mech. and Eng., Vol.195 (2006), pages 3504-3527.
- [15] WHEATLEY V., KUMAR H., HUGUENOT P., *On the Role of Riemann Solvers in Discontinuous Galerkin Methods for Magnetohydrodynamics*, J. Comp. Phys. , Vol 229 (2010), pages 660-680.
- [16] DUBINER, M., *Spectral methods on triangles and other domains*, J. Sci. Comp., Vol. 6 (1991), pages 345-390.
- [17] WARBURTON, T. C. AND KARNIADAKIS, G. E., *A Discontinuous Galerkin Method for the Viscous MHD Equations*, J. Comp. Phys., Vol. 152 (1999), pages 608-641.
- [18] SHU, C. W., *TVD time discretizations*, SIAM J. Math. Anal., Vol. 14 (1988), pages 1073-1084.
- [19] COCKBURN, B. AND SHU, C. W., *The Runge-Kutta local projection  $p^1$ -discontinuous Galerkin method for scalar conservation laws*, M<sup>2</sup>AN, Vol. 25 (1991), pages 337-361.

# Research Reports

No.	Authors/Title
10-49	<i>R. Jeltsch and H. Kumar</i> Three dimensional plasma arc simulation using resistive MHD
10-48	<i>M. Swärd and S. Mishra</i> Entropy stable schemes for initial-boundary-value conservation laws
10-47	<i>F.G. Fuchs, A.D. McMurry, S. Mishra and K. Waagan</i> Simulating waves in the upper solar atmosphere with Surya: A well-balanced high-order finite volume code
10-46	<i>P. Grohs</i> Ridgelet-type frame decompositions for Sobolev spaces related to linear transport
10-45	<i>P. Grohs</i> Tree approximation and optimal image coding with shearlets
10-44	<i>P. Grohs</i> Tree approximation with anisotropic decompositions
10-43	<i>J. Li, H. Liu, H. Sun and J. Zou</i> Reconstructing acoustic obstacles by planar and cylindrical waves
10-42	<i>E. Kokiopoulou, D. Kressner and Y. Saad</i> Linear dimension reduction for evolutionary data
10-41	<i>U.S. Fjordholm</i> Energy conservative and -stable schemes for the two-layer shallow water equations
10-40	<i>R. Andreev and Ch. Schwab</i> Sparse tensor approximation of parametric eigenvalue problems
10-39	<i>R. Hiptmair, A. Moiola and I. Perugia</i> Stability results for the time-harmonic Maxwell equations with impedance boundary conditions
10-38	<i>I. Hnětynková, M. Plešinger, D.M. Sima, Z. Strakoš and S. Van Huffel</i> The total least squares problem in $AX \approx B$ . A new classification with the relationship to the classical works
10-37	<i>S. Mishra</i> Robust finite volume schemes for simulating waves in the solar atmosphere
10-36	<i>C. Effenberger, D. Kressner and C. Engström</i> Linearization techniques for band structure calculations in absorbing photonic crystals